Original Article

Effect of detergent type on the performance of liver decellularized extracellular matrix-based bio-inks

Journal of Tissue Engineering
Volume 12: 1–14

DOI: 10.1177/20417314211997091
journals.sagepub.com/home/tej
SAGE

Wonwoo Jeong*, Min Kyeong Kim* and Hyun-Wook Kang

Abstract

Decellularized extracellular matrix-based bio-inks (dECM bio-inks) for bioprinting technology have recently gained attention owing to their excellent ability to confer tissue-specific functions and 3D-printing capability. Although decellularization has led to a major advancement in bio-ink development, the effects of detergent type, the most important factor in decellularization, are still unclear. In this study, the effects of various detergent types on bio-ink performance were investigated. Porcine liver-derived dECM bio-inks prepared using widely used detergents, including sodium dodecyl sulfate (SDS), sodium deoxycholate (SDC), Triton X-100 (TX), and TX with ammonium hydroxide (TXA), were characterized in detail. SDS and SDC severely damaged glycosaminoglycan and elastin proteins, TX showed the lowest rate of decellularization, and TXA-based dECM bio-ink possessed the highest ECM content among all bio-inks. Differences in biochemical composition directly affected bio-ink performance, with TXA-dECM bio-ink showing the best performance with respect to gelation kinetics, intermolecular bonding, mechanical properties, and 2D/3D printability. More importantly, cytocompatibility tests using primary mouse hepatocytes also showed that the TXA-dECM bio-ink improved albumin secretion and cytochrome P450 activity by approximately 2.12- and 1.67-fold, respectively, compared with the observed values for other bio-inks. Our results indicate that the detergent type has a great influence on dECM damage and that the higher the dECM content, the better the performance of the bio-ink for 3D bioprinting.

Keywords

Bio-ink, decellularization, detergent, 3D bioprinting

Received: 3 February 2021; accepted: 3 February 2021

Introduction

3D bioprinting technology, which can be used to produce biomimetic cellular constructs with multiple cell types, biomaterials, and biomolecules, is extensively utilized in studies of artificial tissue regeneration and disease models. In the 3D-printing process, bio-ink is the most important determinant of micro-patterning, cell viability, functionality, and tissue regeneration. Accordingly, numerous studies have focused on the development of high-performance bio-inks.[1,2] Decellularization, which mostly involves detergent-based processes, is a highly advanced technique for the development of bio-inks with tissue-specific biochemical compositions and has attracted increasing attention.[3] The technique allows the selective removal of cellular components from animal tissues, leaving only the extracellular matrix (ECM). Thus, decellularized ECM-based bio-inks (dECM bio-inks) possess tissue-specific biochemical compositions, which can significantly affect the functions of artificial tissues. Various types of animal tissue-derived dECM bio-inks have been introduced.[4–7] Pati et al.[8] reported that dECM bio-inks derived from the porcine heart, cartilage, and adipose tissue exhibit excellent performance in tissue-specific differentiation. Yi et al.[9] introduced a tumor model printed with glioblastoma-derived dECM bio-ink that produces a patient-specific drug response. Lee et al.[10] reported that liver dECM bio-ink can enhance the function of human hepatic carcinoma cells and the hepatic differentiation of mesenchymal

Department of Biomedical Engineering, Ulsan National Institute of Science and Technology (UNIST), Ulsan, South Korea

*These authors contributed equally to this work.

Corresponding author:
Hyun-Wook Kang, Department of Biomedical Engineering, UNIST, 50, UNIST-gil, Ulsan 44919, South Korea.
Email: hkang@unist.ac.kr

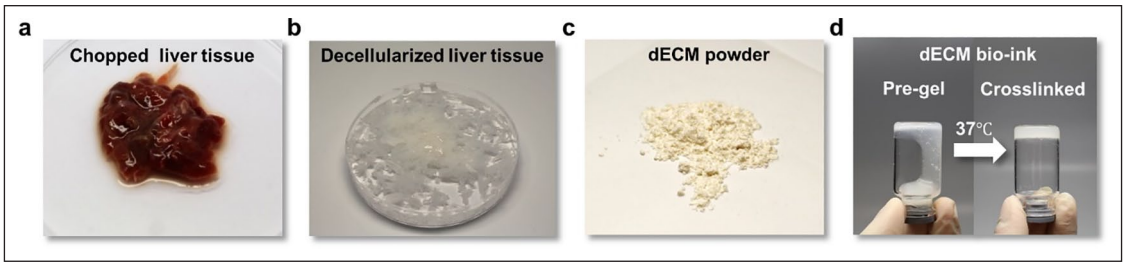

Figure 1. Preparation of liver decellularized extracellular matrix-based bio-inks (dECM bio-inks). Photographs of: (a) chopped porcine liver tissue, (b) decellularized tissue, (c) lyophilized and freezer-milled dECM powder, and (d) pre-gel/thermo-crosslinked dECM bio-ink.

stem cells. These findings demonstrate the various benefits of dECM bio-inks; however, these bio-inks did not show satisfactory performance with respect to their mechanical properties and 3D printability.

Several methods have recently been introduced to enhance the mechanical properties and printability of dECM bio-inks. Výborný et al.[11] and Jang et al.[12] demonstrated that the mechanical properties of dECM bio-inks can be improved by crosslinking with genipin or vitamin. Kim et al.[13] introduced a dECM micro-particle-based bio-ink with enhanced mechanical properties and 3D printability. Choi et al.[14] improved the 3D printability of dECM bio-inks by applying gelatin granules as a temporary support material. Ahn et al.[15] introduced a printing-head module that could simultaneously perform material extrusion and thermal-crosslinking, thereby improving printability. However, the effects of detergents on bio-ink performance have not yet been evaluated. Detergents are not only critical for the decellularization process, but also greatly influence the biological and mechanical properties and printability of dECM bio-inks.[16–18] In this study, the effects of the decellularizing detergents on dECM bio-inks were investigated in a comparative framework. Sodium dodecyl sulfate (SDS), sodium deoxycholate (SDC), Triton X-100 (TX), and TX with ammonium hydroxide (TXA), which are commonly used for decellularization, were applied for the preparation of the dECM bio-inks from porcine livers. The changes in the decellularization efficiency and biochemical composition were evaluated according to the decellularization detergents used. Intermolecular bonding, gelation kinetics, and mechanical properties of the dECM bio-inks were also investigated. Then, 2D and 3D printability were evaluated using an extrusion-based bioprinting system. Finally, cytocompatibility with primary mouse hepatocytes (PMHs) was evaluated to investigate their effects on hepatic function.

Materials and methods

Decellularization process and dECM bio-ink preparation

Porcine livers provided by a slaughterhouse were chopped into 1–2 mm pieces and washed with distilled water to remove debris (Figure 1(a)). SDS (Bioneer, Daejeon, South Korea), SDC (Sigma-Aldrich, MO, St. Louis, USA), and TX (Sigma-Aldrich) detergents were diluted to 0.1% v/v and 1% v/v. TX with ammonium hydroxide (TXA) detergent was prepared by the addition of 0.1% v/v ammonia solution (Samchun, Pohang, South Korea) to 1% v/v TX. Chopped liver tissue was immersed in the detergent solutions, after which the decellularization process was performed at 200 rpm in a shaking incubator at 4°C for 48 h. The detergent solutions were replaced with fresh solutions every 6 h. The detergents were then washed away from the samples (chopped liver tissue) with distilled water (Figure 1(b)). The decellularized liver was prepared as a powder by freeze-drying and milling. (Figure 1(c)). To sterilize the dECM powder, 70% v/v ethyl alcohol (Samchun) was applied for 2 h at 4°C and washed with distilled water. The powder was lyophilized and stored at −20°C until bio-ink preparation. For dECM bio-ink preparation, pepsin (Sigma-Aldrich) solution in 0.1 N HCl (Sigma-Aldrich) was applied to digest the dECM powder (Figure 1(d)). Pepsin (Sigma-Aldrich) at 100 mg per dECM powder weight was used for digestion. Then, the digested dECM solution was adjusted to pH 7.4 with 5 N NaOH solution (Sigma-Aldrich) and supplemented with 10% v/v of 10× PBS. Each bio-ink in the study was prepared at a concentration of 2% w/v. After printing, the prepared dECM bio-ink was thermally crosslinked by incubation at 37°C for 30 min.

Quantification of the biochemical composition of liver dECM

To analyze the decellularization rate, DNA quantification was performed. For digestion, dECM powder was added to a papain solution at a concentration of 10 mg/mL and incubated overnight in a 65°C oven. To prepare the papain solution, 5 mM L-cysteine (Sigma-Aldrich), 100 mM Na_2HPO_4 (Sigma-Aldrich), 5 mM EDTA (Sigma-Aldrich), and 125 μg/mL papain (Sigma-Aldrich) were added to 0.1 N HCl. The Quant-iT PicoGreen dsDNA Assay Kit (Invitrogen, Carlsbad, CA, USA) was used to determine the dsDNA content of the digested solution following the manufacturer's instructions. After sample preparation,

fluorescence intensity was measured using a microplate reader (Synergy Neo2 Hybrid Multi-Mode Reader; BioTek, Winooski, VT, USA) at excitation/emission wavelengths of 360 nm/450 nm. Based on the DNA measurements, sample groups with DNA content less than 50 ng/mg were selected for analyses of the biochemical composition of the dECM.

Glycosaminoglycan (GAG), elastin, and collagen contents were quantified using the Blyscan GAGs Assay Kit (Biocolor Life Sciences, Carrickfergus, UK), Fastin Elastin Assay Kit (Biocolor Life Sciences), and QuickZyme Total Collagen Assay Kit (QuickZime Bioscience, Leiden, Netherland), respectively, according to the manufacturers' instructions. For measuring GAG content, the dECM powder was digested with 10 mg/mL papain solution at 65°C for 18 h. Precipitation was induced by mixing the digested dECM solution and dye reagent with physical shaking for 30 min. After centrifugation and aspiration of the supernatant, the precipitated material was dissolved in 0.5 mL of dissociation reagent. Then, optical density was measured using a microplate reader (SpectraMax Plus 384 Microplate Reader; Molecular Devices, Sunnyvale, CA, USA) at 656 nm. For measuring the collagen content, dECM powder was hydrolyzed with 6 M HCl at a concentration of 100 mg/mL by incubation at 95°C for 20 h. After the dilution of 4 M HCl with distilled water, 35 µL of the hydrolyzed solution was added to a 96-well plate and mixed with 75 µL of assay buffer by shaking for 20 min at room temperature (approximately 20°C). After the addition of 75 µL of detection reagent and incubation at 60°C for 60 min, the sample was cooled to room temperature. Optical density was measured using a microplate reader at 570 nm. For measuring the elastin content, 10 mg of the dECM powder was incubated in 750 µL of 0.25 M oxalic acid at 100°C for 1 h to convert insoluble elastin to soluble α-elastin. After centrifugation, the supernatant was discarded and the procedure was repeated twice to completely dissolve the residual tissues. After mixing with 250 µL of elastin precipitation reagent by vortexing, the solution was incubated at room temperature for 15 min to induce precipitation, and the liquid was drained. Then, the solution was mechanically shaken for 90 min after adding 1 mL of dye reagent. After centrifugation and aspiration of the dye reagent, the sample was mixed with 250 µL of dye dissociation reagent and vortexed for 10 min. Optical density was measured using a microplate reader at 513 nm.

Primary mouse hepatocyte isolation and cell-laden bio-ink preparation

PMHs were isolated from an 8-week-old C57BL/6 mouse by a two-step collagenase method.[19] Briefly, Hank's balanced salt solution (HBSS; Gibco, Grand Island, NY, USA) containing the chelating reagent EDTA was perfused through the inferior vena cava of the mouse. Then, collagenase type I in HBSS was perfused to degrade the liver ECM, and the cell suspensions were filtered through a 70-µm cell strainer. PMHs were separated using a Percoll (Sigma-Aldrich) gradient. Cell viability was evaluated by a trypan blue exclusion test (Gibco) to confirm viability greater than 85%. PMH spheroids were prepared using agarose microwells. A micro-mold (3D Petri Dish®; Merck KGaA, Darmstadt, Germany) was used to prepare the microwells according to the manufacturer's instructions. Briefly, 2% w/v agarose solution (Invitrogen) in saline was heated in a microwave and poured into the micro-mold. After cooling for gelation, the molded agarose microwell was detached and placed in a 12-well plate. Isolated PMHs were then counted and plated in the microwells (256,000 cells/microwell plate), after which PMH spheroid formation was induced by incubating for 48 h at 37°C. Next, spheroids were collected using a 70-µm cell strainer and gently mixed with dECM bio-inks at a concentration of 2000 spheroids/mL. The PMH spheroid-laden dECM bio-ink was loaded in a 1-mL syringe and installed in a mechanical dispenser in the 3D bioprinter. After printing, the PMH spheroids were cultured in William's medium E (Gibco) with hepatocyte maintenance supplements (Thermo Fisher Scientific, Waltham, MA, USA), 10% v/v FBS (Capricorn Scientific GmbH, Ebsdorfergrund, Germany), and 6 µg/mL aprotinin (Sigma-Aldrich). All isolation procedures were approved by the Institutional Animal Care and Use Committee of UNIST (IACUC protocol number: UNISTIACUC-19-23).

Histological analysis

The native and decellularized livers and PMH spheroid-laden bio-inks were fixed in 4% paraformaldehyde (PFA) solution at 4°C overnight, following by a wash step in distilled water. After tissue processing and paraffin embedding, each sample was sectioned at a thickness of 4 µm. Hematoxylin and eosin (H&E) and elastic connective tissue staining were performed according to the manufacturers' instructions. The Elastic Stain Kit (ab150667; Abcam, Cambridge, UK) was used to stain the collagen and elastic fibers. The stained samples were then imaged under a microscope.

Scanning electron microscope (SEM) imaging

The microstructure of 2% w/v dECM bio-inks was investigated using a SEM. Briefly, 100 µL of dECM bio-ink was loaded into a 12-well plate, followed by incubation at 37°C for 30 min to induce thermal crosslinking. After washing with PBS, each bio-ink was fixed with 4% PFA for 1 h at room temperature. Then, samples were washed with distilled water and dehydrated using a graded alcohol series (50%, 70%, 80%, 90%, and 95% v/v alcohol). Dehydrated bio-inks were coated with Pt using a K575X sputter coater

(Quorum Technologies, Lewes, UK) at 15 mA for 45 s and imaged using Cold FE-SEM (SU8220; Hitachi, Tokyo, Japan) at 5 kV and 10 mA.

Measurement of mechanical properties

The rheological properties and compressive modulus of 2% w/v dECM bio-inks were measured. A shear sweep analysis in the range 0.5–50 s^{-1} was conducted to measure the rheological property of 2% w/v dECM bio-inks using a HAAKE MARS III Rheometer (Thermo Fisher Scientific) at 18°C. To measure the storage and loss modulus of the thermal crosslinked dECM bio-ink, a dynamic frequency sweep analysis (1–50 Hz, 2% strain) was conducted using a Kinexus pro+ Rheometer (Malvern Panalytical, Malvern, UK). dECM bio-ink (320 µL) was loaded on the rheometer plate and measured after thermal crosslinking at 37°C for 30 min. A temperature sweep analysis was performed to measure the modulus change of the dECM bio-ink during the thermal crosslinking using the Kinexus pro+ Rheometer (temperature rate of +4°C/min, range 4°C–37°C, 2% strain, and 1 Hz). To measure the compressive modulus of crosslinked dECM bio-inks, cylindrical samples—1 mm in height and 5 mm in diameter—were prepared by punching. The specimen was installed on an Instron machine (Instron Model 3342; Illinois Tool Works Inc., Boston, MA, USA) and slowly compressed at a rate of 1 mm/min. After recording the compression distance and the corresponding force, a stress–strain curve was plotted. The compressive modulus of the crosslinked dECM bio-inks was obtained by calculating the slope of the stress–strain curve at 10% strain.

Swelling behavior analysis

Swelling behavior analysis was performed on lyophilized SDS-, SDC-, and TXA-dECM bio-ink. The samples were weighed and incubated in PBS at 37°C for 15 and 30 min and 1, 2, 4, and 24 h. After collection, excess PBS around the samples was gently wiped off and the samples were immediately weighed. Finally, the swelling ratio was calculated according to the following equation:

$$\text{Swelling ratio}\,(\%) = \frac{W_w - W_d}{W_w} \times 100$$

where W_d indicates the dry weight of the lyophilized dECM bio-inks and W_w indicates the wet weight.

Fourier transform infrared spectroscopy (FT-IR) analysis

The FT-IR was performed to investigate the protein secondary structure of dECM bio-inks. Lyophilized dECM bio-inks were applied to the FT-IR spectrometer (Varian 670-IR; Varian, Palo Alto, CA, USA), and spectra were recorded in the detection range of 600–4000 cm^{-1}. Signals were collected using an attenuated total reflectance crystal detector. All measurements were compared with those of the background spectrum of air. Data were analyzed using Resolutions Pro FTIR (Agilent Technologies, Santa Clara, CA, USA).

Differential scanning calorimetry (DSC)

The DSC (Q200; TA Instruments, New Castle, DE, USA) was performed using the dECM bio-inks. Sample aliquots (10 mg) were hermetically sealed in an aluminum pan and heated at a rate of +10°C/min at a temperature range of 0°C–150°C. A heat flow graph was obtained from the DSC measurements and analyzed using TA Universal Analysis (TA Instruments). The denaturation temperatures (T_d) of the dECM bio-inks were determined during the endothermic process by marking the peak temperature.

Gelation kinetics of the dECM bio-inks

Gelation kinetics of the dECM bio-inks were analyzed turbidimetrically using a UV-VIS spectrometer (SpectraMax Plus 384) at 405 nm. A pre-gel state of 2% w/v dECM bio-ink was prepared at 4°C to inhibit thermal crosslinking. dECM bio-inks (100 µL) were loaded into transparent 96-well plates. To prevent evaporation, other wells were filled with distilled water. The plate reader was pre-heated at 37°C and optical density was measured every 1 min for 90 min. Absorbance values were normalized according to the following equation:

$$\text{NA} = \frac{A - A_0}{A_{max} - A_0}$$

where NA indicates the normalized absorbance, A is the corresponding absorbance, A_0 is the minimum absorbance, and A_{max} is the maximum absorbance.

The half time ($T_{1/2}$) and gelation speed (S) were determined by measuring the time at which the normalized absorbance reached 50% and the maximum slope of the absorbance curve, respectively. Lag time (T_{lag}) was calculated as the intercept with the *x*-axis by extrapolating the linear part of the curve.[20–22]

Printability test

The bio-printing system used in this study consisted of an *XYZ*-axis stage, mechanical dispenser, pneumatic pressure-assisted dispenser, and an enclosure for controlling temperature and humidity (Supplemental Figure S1). The *XY* and *Z* axis stages had resolutions of 250 and 500 nm, respectively. The 3D-printing system was equipped with mechanical dispensers (SMP-III; Musashi Engineering Inc., Tokyo, Japan) and a pneumatic pressure controller

(ML-808GX; Musashi) with a heating unit (TCD-200; Musashi Engineering Inc.) to print bio-ink and thermoplastics. After loading 2% w/v dECM bio-ink into a 1-mL syringe connected to a 300-μm nozzle, the syringe was installed in a mechanical dispenser. Then, a printability test was performed by changing the printing speed and pattern at a dispensing rate of 0.5735 μL/s. First, a line pattern of 2% w/v dECM bio-ink was extruded at a printing speed of 5–200 mm/min according to the detergent. Images of the printed line were obtained using a microscope, and the line width and height were measured using ImageJ (NIH, Bethesda, MD, USA). The aspect ratio was calculated by dividing the measured line height by the width of the dECM bio-ink.

The 2D and 3D printability were evaluated by grid patterns and stacking tests. Grid patterns with 600–1000-μm pores were printed at 30 mm/min, and images of the fabricated patterns were obtained under a microscope. After measuring the pore area using ImageJ, the pore fidelity was calculated using the following equation:

$$\text{Pore fidelity}\,(\%) = \frac{Printed\ \ pore\ area}{Designed\ \ pore\ area} \times 100$$

Finally, for the stacking test, 1-, 4-, 7-, and 10-layered square structures were printed at a printing speed of 30 mm/min and layer thickness of 150 μm. After printing the designed structure, images of the side view were acquired under a microscope, and the printed height was measured using ImageJ.

Cytocompatibility test

Cytocompatibility was evaluated by performing cell viability, metabolic activity, cytochrome P450 (CYP) activation, albumin, and urea assays using 2% w/v dECM bio-inks. After printing the PMH spheroid-laden dECM bio-ink, it was thermally crosslinked in an incubator at 37°C for 30 min. Cell viability was evaluated using the Live/Dead Cell Viability Assay Kit (L-3224; Life Technologies, Carslbad, CA, USA) on days 1 and 14. After washing with PBS twice, the samples were stained with 0.5 μL/mL calcein-AM and 2 μL/mL ethidium homodimer-1 in PBS at room temperature for 1 h. Then, the staining results were observed and images were acquired using a DM2500 fluorescence microscope (Leica, Wetzlar, Germany). After counting live and dead cells using ImageJ, cell viability was calculated by dividing the number of live cells by the total number of cells. To measure the metabolic activity of the PMH spheroids in dECM bio-inks, intracellular ATP levels were measured using the CellTiter-Glo 3D Cell Viability Assay kit (G9683; Promega, Madison, WI, USA) according to the manufacturer's instructions. Briefly, 50% CellTiter-Glo 3D reagent solution was prepared with the culture medium and 200 μL of the reagent solution was added to the PMH spheroid-laden dECM bio-inks. Then, the samples were incubated for 30 min at room temperature and aliquots (100 μL) were collected into 96-well plates. Luminescence was then measured using a multi-mode microplate reader (Biotek). To evaluate the CYP activation of the PMH spheroids, luminescence was measured using the CYP1A2 Assay Kit (P450-Glo; Promega) according to the manufacturer's instructions. Briefly, the CYP activation of cell-laden samples was induced with 2 μM of 3-methylchoranthrene (3MC) in the culture medium for 48 h, and the medium was exchanged every 24 h. Samples in the uninduced group were treated with DMSO. For the reaction, 0.5 μM Luciferin1A2 solution with 3 mM salicylamide (Sigma-Aldrich) in PBS was added to each sample. Samples were incubated at 37°C for 30 min, after which 25 μL of the Luciferin1A2 solution was transferred into 96-well plates. Then, 25 μL of luciferin detection reagent was added to the wells and reacted at room temperature for 20 min. A microplate reader was used to measure luminescence. To evaluate albumin and urea secretion, the printed bio-inks were incubated for 24 h after exchanging with fresh culture medium. After sampling the culture medium, albumin and urea contents were measured using the Albumin ELISA Kit (Koma Biotech, Seoul, South Korea) and QuantiChrom Urea Assay Kit (BioAssay Systems, Hayward, CA, USA), respectively, according to the manufacturers' instructions. In brief, for albumin measurement, 100 μL of culture medium was added to a 96-well plate coated with a goat anti-mouse albumin antibody. Thereafter, the HRP-conjugated detection antibody was added to each well, followed by treatment with TMB solution for color development. The absorbance of albumin was measured at a wavelength of 450 nm using a microplate reader. For measuring urea secretion, 200 μL of urea detection reagent and 50 μL of culture medium were mixed in a 96-well plate and incubated at room temperature for 50 min. Absorbance was measured at 480 nm using a microplate reader.

Statistical analysis

All values are expressed as means ± standard deviation. Significant differences between the experimental groups were analyzed using one-way ANOVA and Tukey's multiple comparison tests. In all analyses, $p < 0.05$ was considered statistically significant.

Results

Characterization of liver dECMs

DNA content of the liver dECMs decellularized with SDS, SDC, TX, and TXA were measured (Figure 2). Regardless of the detergent type, DNA content decreased exponentially as the process time increased, with a rate of reduction that increased in the order TX < SDC < TXA < SDS. The

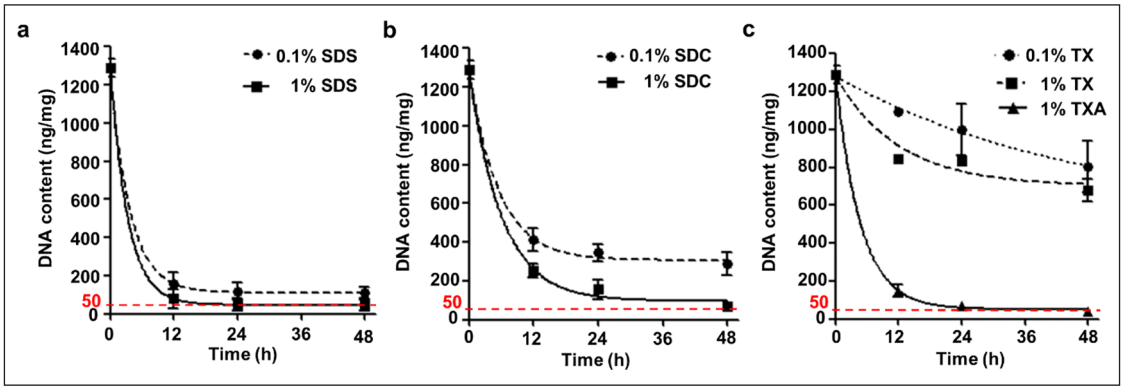

Figure 2. Quantification of the DNA content of dECM according to detergent type. DNA content of dECM at various processing times and concentrations using: (a) SDS, (b) SDC, (c) Triton X-100 (TX), and Triton X-100 with ammonium hydroxide (TXA). Red dotted lines indicate a DNA concentration of 50 ng/mg. All experiments were repeated three times ($n = 5$).

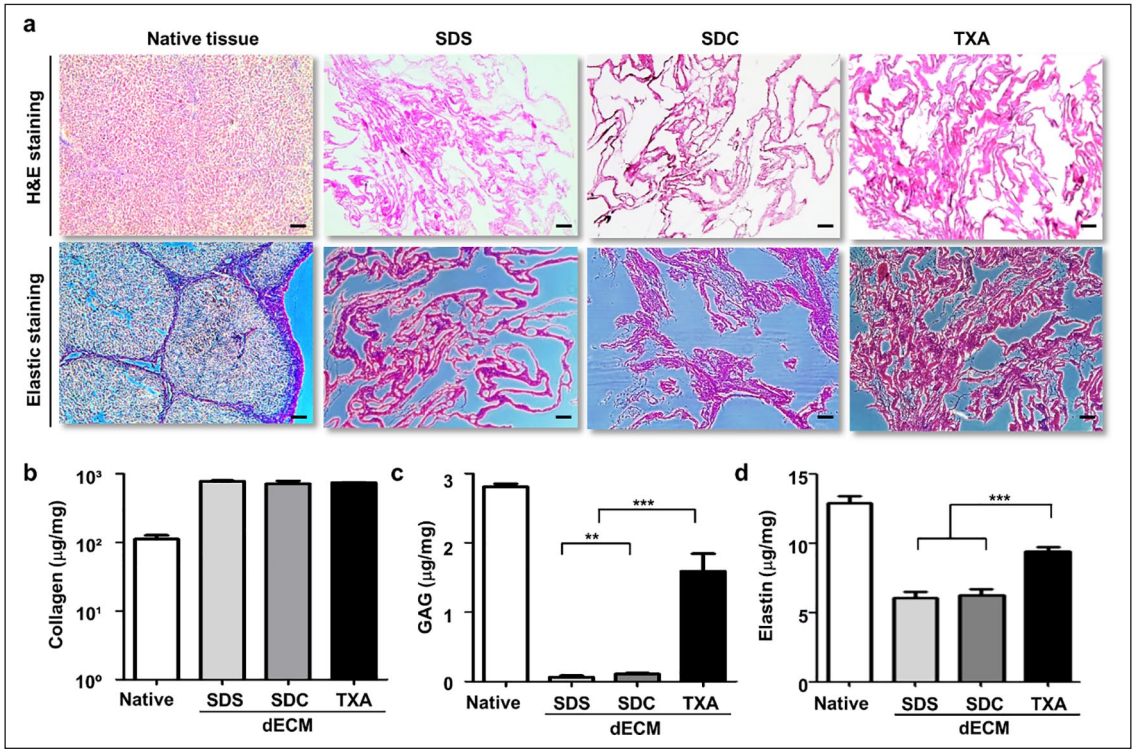

Figure 3. Histological and biochemical assays of the decellularized tissues. (a) H&E and elastin staining of native liver and decellularized tissues processed with SDS, SDC, and TXA. Collagen, red; elastic fibers, blue. Scale bars: 200 μm. Measured collagen (b), GAG (c), and elastin (d) contents in the tissues. Error bars represent standard deviations ($n = 5$; $^{**}p < 0.005$; $^{***}p < 0.001$).

1% v/v SDS, TXA, SDC, and TX groups showed 94%, 89%, 81%, and 35% reduction in DNA content, respectively, at 12 h. DNA content of the 1% v/v SDS group decreased to less than 50 ng/mg in 24 h, while the 1% v/v SDC and TXA groups required 48 h to reach similar DNA levels. In the TX group, the DNA content did not reach 50 ng/mg, even after 2 days. Based on these results, 1% v/v SDS (24 h), SDC (48 h), and TXA (48 h) were used for further experiments.

Histological analysis and biochemical assay results are summarized in Figure 3. As determined by H&E staining, only the ECM structure was observed in the dECM groups and no cells were observed (upper panels in Figure 3(a)). In the SDS and SDC groups, collagen was mainly observed, while elastic fibers were rarely detected (lower panels in Figure 3(a)). The elastic fiber content was highest in the TXA group. Similar trends were observed upon the quantitative analysis of the ECM proteins (Figure 3(b)–(d)). As

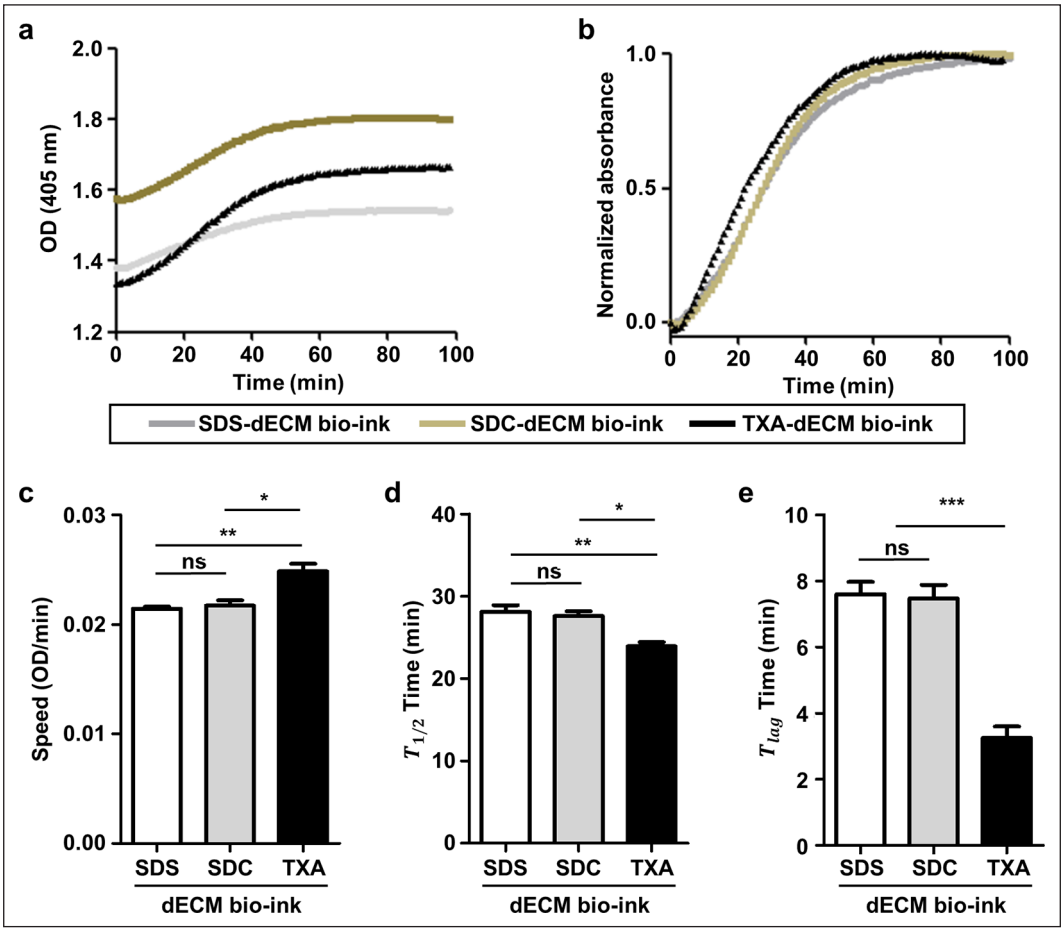

Figure 4. Gelation kinetics of 2% w/v dECM bio-inks. Representative (a) and normalized (b) turbidimetric gelation kinetics (wavelength, 405 nm) of SDS-, SDC-, and TXA-dECM bio-inks. Crosslinking speed (c), $T_{1/2}$ (d), and T_{lag} (e). Speed represents the rate of crosslinking, and $T_{1/2}$ is the time to achieve 50% crosslinking. T_{lag} is the delay until the initiation of crosslinking. Error bars represents standard deviations ($n = 5$; ns: no significance; *$p < 0.05$; **$p < 0.005$; ***$p < 0.001$).

shown in Figure 3(b), all dECM groups had a collagen content that was approximately 6.4–7-fold higher than that of the native liver tissue, but the difference among the groups was not significant. Different trends were observed for GAG and elastin content (Figure 3(c) and 3(d)), which decreased by 98% and 54%, respectively, in the SDS and SDC groups compared with native liver tissue. In the TXA group, the decrease in the dECM protein content occurred at a lesser extent while GAG and elastin contents was maintained at levels approximately 4.22- and 1.5-fold higher than those of the other two groups, respectively.

Turbidimetric gelation kinetics of dECM bio-inks

Thermal crosslinking kinetics of 2% w/v SDS-, SDC-, and TXA-dECM bio-inks were investigated by measuring the turbidity using a spectrometer (Figure 4). Figure 4(a) and 4(b) show the measured optical density and normalized values, respectively. Speed, $T_{1/2}$, and T_{lag} were calculated from the plot of the normalized values (Figure 4(c)–(e)), where speed represents the rate of crosslinking, $T_{1/2}$ is the time to achieve 50% crosslinking, and T_{lag} indicates the delay in time after the initiation of crosslinking by temperature. The TXA-dECM bio-ink had the fastest crosslinking speed with the lowest $T_{1/2}$ and T_{lag} values among the dECM bio-inks. Differences among the bio-inks were significant; in particular, T_{lag} values for the SDC- and SDC-dECM groups were about 2.3-fold lower than those of the TXA-dECM group. No significant difference in gelation kinetics was observed between the SDS- and SDC-dECM bio-inks.

Analysis of intermolecular bonding

The FT-IR analysis was performed to investigate the secondary protein structures of the liver dECM bio-inks (Figure 5(a)). SDS-, SDC-, and TXA-dECM bio-inks had similar compositions but large differences in peak intensities. In all groups, absorption bands indicating C=O and

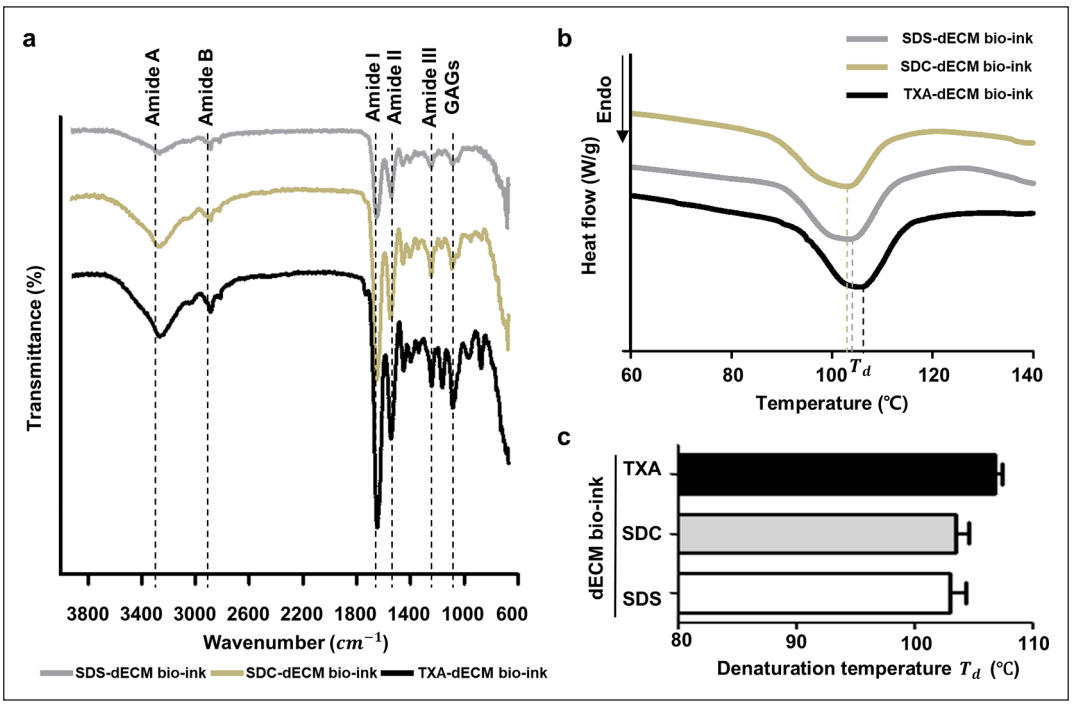

Figure 5. The FT-IR spectra and thermal analysis results of dECM bio-inks. Representative FT-IR spectra (a), DSC thermogram (b), and temperature peaks (T_d) during collagen fiber denaturation (c) of SDS-, SDC-, and TXA-dECM bio-inks. Error bars represent standard deviations ($n = 3$).

N–H stretching of peptides were observed for the amide A (3307 cm^{-1}) and amide B (2927 cm^{-1}) peaks, respectively.[23,24] Amide I (1654 cm^{-1}), amide II (1548cm^{-1}), and amide III (1238cm^{-1})—referred to as the collagen fingerprint—and glycosaminoglycan (1048 cm^{-1}) peaks were also observed.[25,26] TXA-dECM bio-inks had the largest peaks, and the intensities decreased in the order TXA- > SDC- > SDS-dECM bio-inks. Figure 5(b) and (c) show the DSC results for the crosslinked dECM bio-inks. SDS- and SDC-dECM bio-inks started the endothermic process at approximately 91°C and had similar denaturation temperature peaks (T_d) at approximately 103.8°C and 104.3°C, respectively. For the TXA-dECM bio-ink, the endothermic process began at approximately 93°C, and its denaturation temperature was the highest (approximately 107.72°C) compared with that of the other bio-inks.

Mechanical properties and microstructures of the dECM bio-inks

Mechanical properties and microstructures of the SDS-, SDC-, and TXA-dECM bio-inks were analyzed (Figure 6). The TXA-dECM bio-ink possessed the highest viscosity, which was approximately 4.05–22.61-fold higher than that of the others. Moreover, shear thinning effects were observed for all groups, that is, the viscosity decreased as the shear rate increased (Figure 6(a)).

Figure 6(b) shows the results of a dynamic frequency sweep analysis of thermal-crosslinked dECM bio-inks. In all groups, the storage modulus was higher than the loss modulus in the frequency range, indicating that the hydrogel was effectively maintained under dynamic conditions. The TXA-dECM bio-ink had the highest storage modulus (G′), which was approximately 24%–70% higher than that of others. The storage modulus of the SDC group was approximately 5%–33% higher than that of the SDS group. Figure 6(c) shows the results of the thermal sweep analysis. Overall, the modulus increased with temperature in all groups; in particular, a sharp increase was observed around 37°C and the TXA-dECM bio-ink had the highest modulus. Next, we imaged the three dECM bio-inks via SEM and found that they were composed of nano-fibers with the TXA group showing the most compact structure (Figure 6(d)). Swelling behavior of the dECM bio-inks was also investigated (Supplemental Figure S3); all groups had a tendency to saturate after the swelling ratio increased during the initial 2 h. Moreover, the higher the nano-fiber packing density in the microstructure, the higher the swelling ratio. Thus, the TXA-dECM bio-ink group had the highest swelling ratio of approximately 93%, while the SDS group had the lowest value (approximately 89%; TXA- vs SDS-dECM bio-ink, $p = 0.077$). Consistent with these findings, the compression test demonstrated that the TXA-dECM bio-ink had the highest modulus (i.e. 3.45 kPa) among all groups, which was 2.6- and 5.89-fold

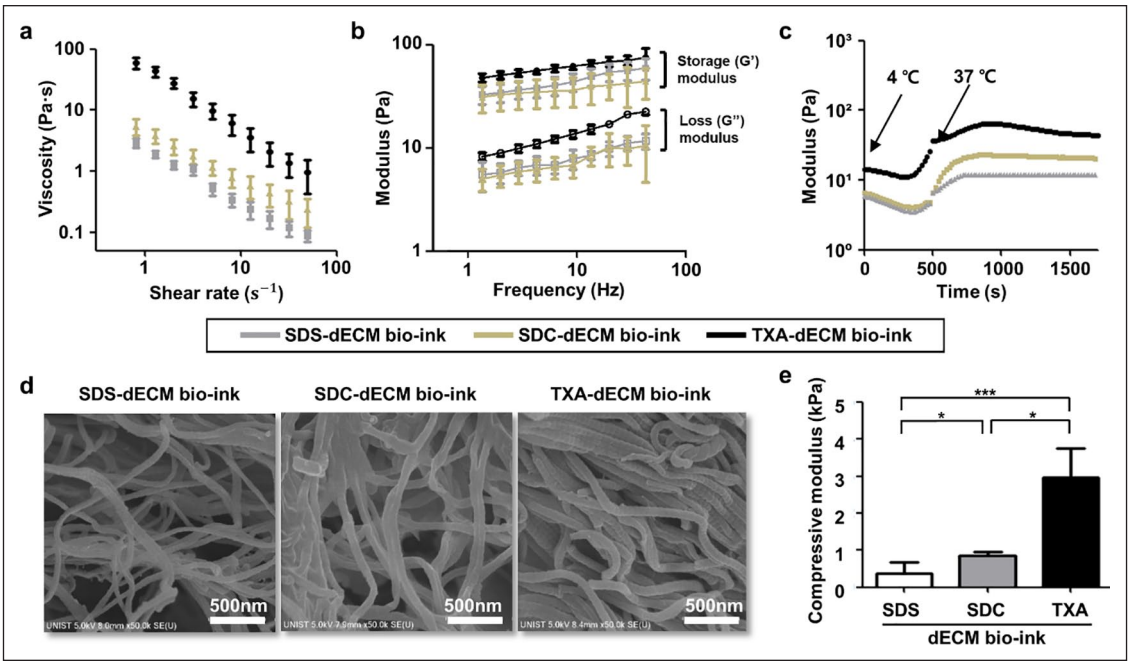

Figure 6. Mechanical properties and microstructure of dECM bio-inks. Shear sweep (a), dynamic frequency sweep (b), and thermal sweep (c) analysis results of 2% w/v SDS-, SDC-, and TXA-dECM bio-inks. SEM images (d) and the compressive modulus (e) of the bio-inks.
Error bars represent standard deviations ($n = 3$; *$p < 0.05$; ***$p < 0.001$).

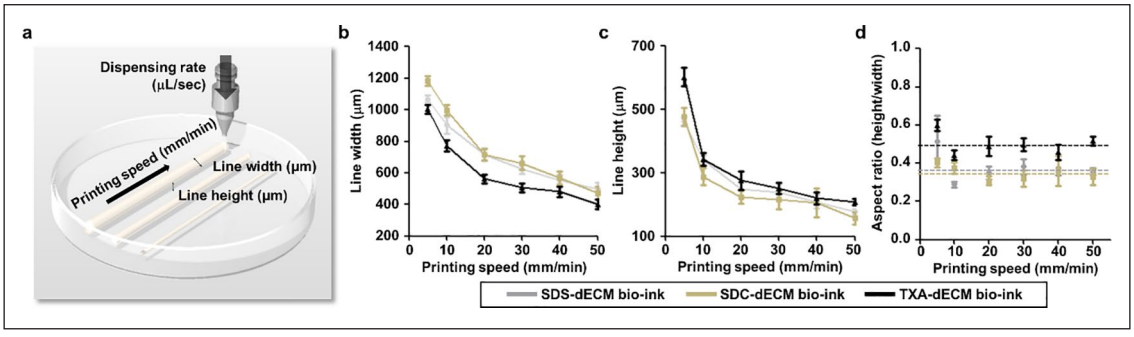

Figure 7. Printing results for dECM bio-inks. (a) Schematic illustration of the line patterning test. Measured widths (b) and heights (c) of the lines printed with 2% w/v SDS-, SDC-, and TXA-dECM bio-inks with various printing speeds. (d) Corresponding aspect ratios of the line patterns calculated by dividing heights by widths.
Dotted lines indicate the saturation points of the aspect ratios as the printing speed increased. Error bars represent standard deviations ($n = 3$).

higher than that of the SDC- and SDS-dECM bio-inks, respectively (Figure 6(e)).

2D and 3D printability of the dECM bio-inks

The 2D and 3D printing tests were conducted to evaluate the printability of the three types of dECM bio-inks. After line patterns were printed with a 300-μm nozzle at a dispensing rate of 0.5735 μL/s, the line width and height were measured (Figure 7(a)). Line width and height decreased exponentially as the printing speed increased for all groups (Figure 7(b) and (c)). In the TXA group, continuous line patterns were generated up to a speed of 80 mm/min and a disconnected line pattern was produced at a printing speed of 100 mm/min (Supplemental Figure S2). The minimum line width achievable with the TXA-dECM bio-ink was approximately 290.15 μm under the applied conditions. In the SDS and SDC groups, disconnected lines were observed from 80 mm/min and the minimum widths were 497.9 ± 42.34 and 474.95 ± 40.61 μm, respectively. Based on the measurement results, aspect ratios were calculated (Figure 7(d)), which converged to a specific value as the printing speed increased. Among the three groups, the TXA-dECM bio-ink had the highest aspect ratio of 0.4817, which was 1.37–1.45-fold higher than that of the others.

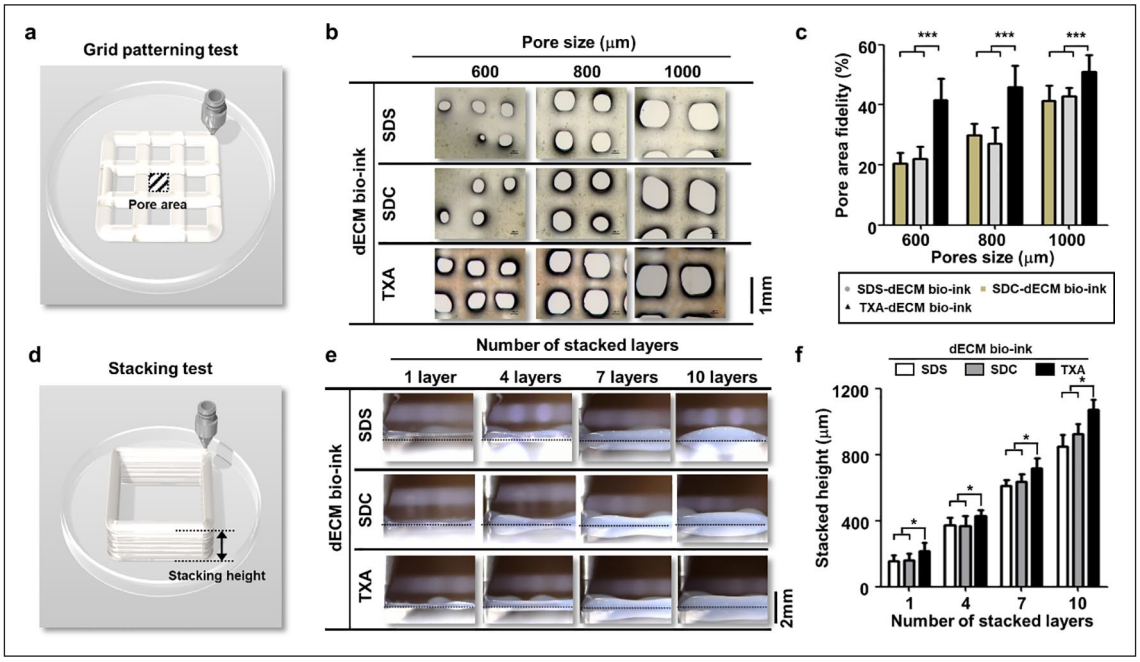

Figure 8. 2D and 3D printability of dECM bio-inks. Schematic illustrations and optical images of the printing results of the grid patterning ((a), (b)) and stacking ((d), (e)) tests. The printability test was conducted with 2% w/v SDS-, SDC-, and TAX-dECM bio-inks and the results are presented according to the pore size and the number of stacked layers. Pore area fidelity (c) and stacked height (f) were measured from the optical images (b) and (e), respectively.
Error bars represent standard deviations ($n = 3$; $^{*}p < 0.05$; $^{***}p < 0.001$).

The 2D and 3D printability test results were consistent with those of the line printing test (Figure 8). For the 2D printability test, a grid pattern with a 600–1000-μm pore size was printed, and the fabricated pore area was measured (Figure 8(a) and 8(b)). In all groups, the pore area fidelity improved as the pore size increased (Figure 8(c)); the TXA-dECM bio-ink group achieved the best performance in the grid patterning test and showed approximately 1.89–2.03-fold greater fidelity than that of the others during printing with a 600-μm pore size. A stacking test was then conducted to evaluate the 3D printability of the dECM bio-inks (Figure 8(d)). A ten-layered structure was well fabricated with the TXA-dECM bio-ink but the structure collapsed and the edges were rounded in the SDC and SDS groups (Figure 8(e)). The stacking height of the TXA group was significantly higher (by approximately 15%–25%) than that of the other groups (Figure 8(f)).

Cytocompatibility of the dECM bio-inks

PMH spheroids were used for a cytocompatibility test of the liver dECM bio-inks. A collagen (COL) group was used as the control. H&E staining demonstrated that the PMH spheroids of all groups were maintained in a cluster form for 14 days (Figure 9(a)). The TXA and COL groups had a cell viability $> 80\%$ during the 2-week period, whereas the SDC and SDS groups had relatively low cell viabilities (70% and 40%, respectively) (Figure 9(b)). The metabolic activity results slightly differed from the live/dead assay results (Figure 9(b) and Supplemental Figure S4). In all groups, the metabolic activity of PMH in the dECM bio-inks gradually decreased over time, with the TXA- and SDC-dECM bio-ink groups showing the highest activity and the SDS group, the lowest, for 14 days; these differences were statistically significant. On day 7 of cultivation, the TXA group had the highest CYP activity, which was about 1.67- and 2.89-fold higher than that of the COL and SDC groups, respectively (Figure 9(c)). Albumin and urea secretory functions of the embedded PMH spheroids were also evaluated (Figure 9(d) and 9(e)); the TXA group showed the highest albumin secretion, but a gradually decreasing trend in secretion was observed in all groups; on day 13, the TXA-dECM bio-ink group maintained albumin secretion at about 45% of the level observed on day 1, while only 20% was maintained by the COL, SDS, and SDC groups. Similarly, the TXA group showed the highest urea secretion, and all groups exhibited a decreasing trend over time (Figure 9(e)). In the TXA group, urea secretion was maintained at about 38.95% on day 13 compared to the day 1 levels and was significantly different compared with that of the COL and SDS groups. The SDS group showed the greatest decrease in urea secretion, dropping to only 22% on day 13.

Discussion

Various types of dECM bio-inks have been introduced for potential applications in artificial tissue regeneration.[5–10]

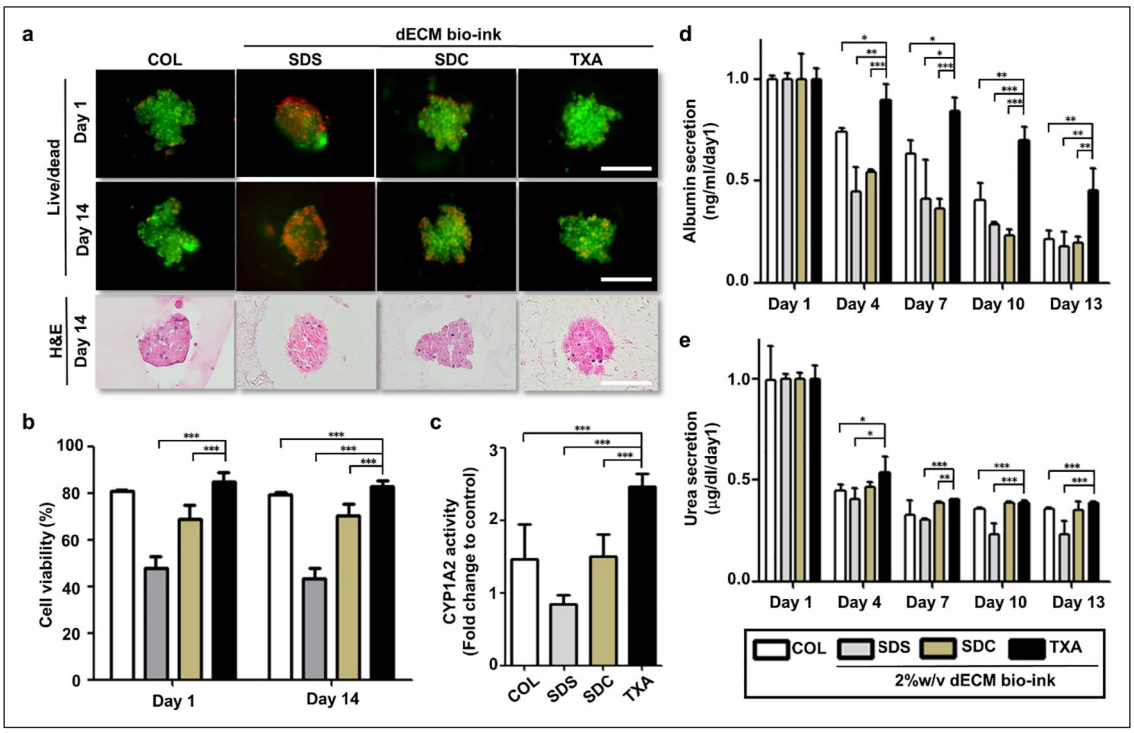

Figure 9. Cytocompatibility of the dECM bio-inks with primary mouse hepatocytes (PMHs). (a) Live/dead assay and H&E staining results of PMH spheroids in 2% w/v collagen hydrogel (COL; control) and SDS-, SDC-, and TXA-dECM bio-inks on days 1 and 14. Cell viability (b), CYP1A2 activity (c), and albumin (d) and urea (e) secretion assays. CYP1A2 activation was induced by 3-methylcholanthrene and measured on day 7.
Error bars represent standard deviations ($n = 5$; *$p < 0.05$; **$p < 0.01$; ***$p < 0.001$).

In dECM bio-ink development, detergents are commonly used in the decellularization process and are the greatest determinants of the bio-ink properties.[16–18,20–22] Despite various studies on dECM bio-inks, analyses of the effectiveness of different detergents are lacking. In this study, the effects of various detergents on the biochemical composition, mechanical properties, printability, and cytocompatibility of dECM bio-inks were investigated. Liver dECM bio-inks were prepared with common detergents used for the decellularization process, namely SDS, SDC, TX, and TXA, and the characteristics of the bio-inks were evaluated. We found that TXA was the most suitable detergent for the preparation of liver dECM bio-inks. Interestingly, TX alone cannot achieve sufficient decellularization, but adding ammonium hydroxide allowed us to achieve a high decellularization rate with ECM retention. Indeed, TXA-dECM possessed the highest dECM protein content and showed the best performance in terms of gelation kinetics, intermolecular interactions, mechanical properties, and 2D/3D printability. Furthermore, the bio-ink effectively sustained the viability and hepatic functions of PMHs.

In this study, we used SDS-, SDC-, and TXA-dECM bio-inks for the subsequent analysis as they achieved DNA concentrations below 50 ng/mg; this concentration is widely used as a reference for successful decellularization.[3] Although the ionic detergents SDS and SDC enabled rapid decellularization, they severely damaged the ECM (Figures 2 and 3). The non-ionic detergent TX resulted in a very low rate of decellularization as it was unable to reduce DNA content past 50% even after decellularization for more than 2 days. However, we confirmed that the incorporation of the ammonia solution with TX greatly improved the decellularization rate. TXA enabled not only rapid decellularization but also a high rate of ECM protein retention. The TXA rate of decellularization was lower than that of SDS but faster than that of SDC (Figure 2). The physical properties likely resulted in the generation of a hypertonic environment around the liver tissue due to the presence of ammonium[27]; this difference in osmotic pressure improved the efficiency of decellularization. Fresh liver- and TX-dECM could not be prepared as cross-linkable bio-inks, as they contained a high content of cellular components. Moreover, collagen was largely retained in all groups, regardless of the detergent type. Collagen content of the dECM materials was higher than that of the native tissue because collagen content is expressed in concentration and cellular components were removed from the native tissues. Similar trends have frequently been reported in decellularization studies.[28,29] On the other hand, the GAG and elastin contents showed a different trend, with a particularly large difference in GAG; this is because GAG is a soluble component and is easily damaged depending on the detergent type.[29,30] Based on these

results, we found that GAG content is very important for evaluating the dECM protein retention rate.

TXA-dECM bio-ink retaining high ECM protein levels showed the best performance with respect to intermolecular bonding, gelation kinetics, and mechanical properties, among the prepared bio-inks. The ECM of tissues consists mainly of fibrous networks (such as collagen and elastic fibers) and macromolecules (such as proteoglycans), and the ECM network is formed by interactions between these components. Therefore, such components have a great influence on the gelation characteristics and mechanical properties of dECM bio-inks.[31–33] Indeed, the difference in GAG content affected the gelation kinetics, with the TXA-dECM bio-ink exhibiting the fastest gelation speed, even though all bio-inks had similar collagen content. This is because GAG enhances collagen crosslinking[34] and promotes coacervation for the formation of elastin fiber.[35,36] The GAG and elastin content also substantially influenced the mechanical properties of the dECM bio-inks, and the TXA group showed the highest viscosity and moduli. Similarly, Kalbitzer et al.[37] reported that GAGs influence collagen fibril formation and improve mechanical properties. Henninger et al.[38] also reported a 60%–70% reduction in the modulus of ligament tissue by the selective removal of elastin. Moreover, analysis of the secondary protein structures by FT-IR demonstrated that TXA-dECM bio-inks with high GAG and elastin contents had a significantly enhanced amide bonding compared with that of other inks, with broad and intense amide A and amide B peaks corresponding to the O-H stretching vibration. This indicates that a large number of hydrogen bonds were formed in the bio-ink, thereby improving molecular interactions with proteins.[39,40] DSC thermal analysis also showed that the TXA-dECM bio-ink had the highest denaturation temperature. In fact, Samouillan et al.[41] reported that elastin and GAGs induce an entropic effect, increasing the fiber packing density. Based on these results, we confirmed that GAG and elastin content greatly influences the intermolecular bonding, gelation kinetics, and mechanical properties of dECM bio-inks.

The TXA-dECM bio-ink also showed a high conservation of ECM proteins and had excellent 2D and 3D printability. Ouyang et al.[42] reported that the rheological properties of bio-inks have critical roles in cell viability and the integrity of the printed structure. As the TXA-dECM bio-ink had the highest viscosity, it showed the best resolution, line patterning, 2D patterning, and 3D stacking results. In particular, a striking difference was observed in the 3D printability stacking test; the SDS- and SDC-dECM bio-ink-printed structure collapsed during layering (Figure 8(e)), whereas that of the TXA-dECM bio-ink was maintained at 10 layers. Structure collapse during layering is closely related to the viscosity of dECM bio-inks; the lower the viscosity, the more difficult it is to maintain the printed structure.[43] Accordingly, the structure collapse was the most severe for the SDS group as it had the lowest viscosity.

The ECM content significantly influenced the viability and hepatic function of PMHs. As the TXA-dECM bio-ink had the highest ECM content, it showed the best cytocompatibility (Figure 9). For the SDS-dECM bio-ink, low cell viability and metabolic activity were observed from the beginning of the culture period, and hepatocyte function was severely reduced. White et al.[16] reported that SDS fragments remaining in dECM can induce cell lysis. In this study, SDS-dECM was vigorously washed for 7 days to completely remove SDS; however, retention of SDS remnants is possible. Moreover, the relatively low ECM content in SDS-dECM affected hepatic function. Overall, the TXA-dECM bio-ink group outperformed the control group with respect to CYP activity and albumin secretion. In conclusion, TXA provided the best environment for primary hepatocyte culture among the detergents used for dECM bio-inks. The superior performance of TXA-dECM bio-inks across the board can be explained by the ECM protein content as well as the crucial biomolecules that have not yet been identified.

Conclusion

We investigated the effects of various detergent types on liver dECM bio-inks and 3D bioprinting. Liver tissue was employed owing to its high cell density and sensitivity to the decellularization process, but further studies on a variety of different tissue types are needed. dECM bio-inks were prepared using SDS, SDC, TX, and TXA as they are the most widely used detergents in the decellularization process. The detergent type had significant effects on the biochemical composition of the dECM, its cytocompatibility, as well as 2D/3D printability. The TXA-dECM bio-ink had the highest ECM content, conferring improved molecular interactions, gelation kinetics, printability, and cytocompatibility. Therefore, we confirmed that TXA detergent is the most suitable for the preparation of liver dECM bio-inks. Nevertheless, further studies are needed to increase the gelation rate of dECM bio-inks by applying synthetic polymers or crosslinking agents to improve 3D printability. Overall, our findings provide a basis for the development of various dECM bio-inks with excellent performance for 3D bioprinting and tissue engineering.

Declaration of conflicting interests

The author(s) declared no potential conflicts of interest with respect to the research, authorship, and/or publication of this article.

Funding

The author(s) disclosed receipt of the following financial support for the research, authorship, and/or publication of this article: This research was supported by the National R&D Program

through the National Research Foundation of Korea (NRF) funded by the Ministry of Science and ICT (No. NRF-2020M3H4A1A02084827 and NRF-2020R1F1A1075865) and the Leading Foreign Research Institute Recruitment Program (No. NRF-2018K1A4A3A01063890) through the National Research Foundation of Korea funded by the Ministry of Education, Science and Technology (MEST).

ORCID iD

Hyun-Wook Kang https://orcid.org/0000-0001-5335-5604

Supplemental material

Supplemental material for this article is available online.

References

1. Sun W, Starly B, Daly AC, et al. The bioprinting roadmap. *Biofabrication* 2020; 12(2): 022002.
2. Ozbolat IT, Moncal KK and Gudapati H. Evaluation of bioprinter technologies. *Addit Manuf* 2017; 13: 179–200.
3. Crapo PM, Gilbert TW and Badylak SF. An overview of tissue and whole organ decellularization processes. *Biomaterials* 2011; 32(12): 3233–3243.
4. Sellaro TL, Ranade A, Faulk DM, et al. Maintenance of human hepatocyte function in vitro by liver-derived extracellular matrix gels. *Tissue Eng Part A* 2010; 16(3): 1075–1082.
5. Das S, Kim S-W, Choi Y-J, et al. Decellularized extracellular matrix bioinks and the external stimuli to enhance cardiac tissue development in vitro. *Acta Biomaterialia* 2019; 95: 188–200.
6. Pati F, Ha D-H, Jang J, et al. Biomimetic 3D tissue printing for soft tissue regeneration. *Biomaterials* 2015; 62: 164–175.
7. Yun H-W, Choi BH, Park DY, et al. Inhibitory effect of topical cartilage acellular matrix suspension treatment on neovascularization in a Rabbit Corneal Model. *Tissue Eng Regen Med* 2020; 17(5): 625–640.
8. Pati F, Jang J, Ha D-H, et al. Printing three-dimensional tissue analogues with decellularized extracellular matrix bioink. *Nat Commun* 2014; 5: 3935.
9. Yi H-G, Jeong YH, Kim Y, et al. A bioprinted human-glioblastoma-on-a-chip for the identification of patient-specific responses to chemoradiotherapy. *Nat Biomed Eng* 2019; 3: 509–519.
10. Lee H, Han W, Kim H, et al. Development of liver decellularized extracellular matrix bioink for three-dimensional cell printing-based liver tissue engineering. *Biomacromolecules* 2017; 18: 1229–1237.
11. Výborný K, Vallová J, Kočí Z, et al. Genipin and EDC crosslinking of extracellular matrix hydrogel derived from human umbilical cord for neural tissue repair. *Sci Rep* 2019; 9: 10674.
12. Jang J, Kim TG, Kim BS, et al. Tailoring mechanical properties of decellularized extracellular matrix bioink by vitamin B2-induced photo-crosslinking. *Acta Biomater* 2016; 33: 88–95.
13. Kim MK, Jeong W, Lee SM, et al. Decellularized extracellular matrix-based bio-ink with enhanced 3D printability and mechanical properties. *Biofabrication* 2020; 12: 025003.
14. Choi Y-J, Jun Y-J, Kim DY, et al. A 3D cell printed muscle construct with tissue-derived bioink for the treatment of volumetric muscle loss. *Biomaterials* 2019; 206: 160–169.
15. Ahn G, Min KH, Kim C, et al. Precise stacking of decellularized extracellular matrix based 3D cell laden constructs by a 3D cell printing system equipped with heating modules. *Sci Rep* 2017; 7: 1–11.
16. White LJ, Taylor AJ, Faulk DM, et al. The impact of detergents on the tissue decellularization process: a ToF-SIMS study. *Acta Biomater* 2017; 50: 207–219.
17. Haupta J, Paura A and Habena I. Detergent-based decellularization strategy preserves macro- and microstructure of heart valves. *Interact Cardiovasc Thorac Surg* 2018; 26: 230–236.
18. Youngstrom DW, Barrett JG, Jose RR, et al. Functional characterization of detergent-decellularized equine tendon extracellular matrix for tissue engineering applications. *PLoS One* 2013; 8: e64151.
19. Seglen PO. Preparation of isolated rat liver cells. *Methods Cell Biol* 1976; 13: 29–83.
20. Fernández-Pérez J and Ahearne M. The impact of decellularization methods on extracellular matrix derived hydrogels. *Sci Rep* 2019; 9: 1–12.
21. Freytes DO, Martin J, Velankar SS, et al. Preparation and rheological characterization of a gel form of the porcine urinary bladder matrix. *Biomaterials* 2008; 29: 1630–1637.
22. Wolf MT, Daly KA, Brennan-Pierce EP, et al. A hydrogel derived from decellularized dermal extracellular matrix. *Biomaterials* 2012; 33: 7028–7038.
23. Ventura RD, Padalhin AR, Park CM, et al. Enhanced decellularization technique of porcine dermal ECM for tissue engineering applications. *Mater Sci Eng C* 2019; 104: 1–12.
24. Riaz T, Zeeshan R, Zarif F, et al. FTIR analysis of natural and synthetic collagen. *Appl Spectrosc Rev* 2018; 53: 703–746.
25. Efraim Y, Schoen B, Zahran S, et al. 3D structure and processing methods direct the biological attributes of ECM-based cardiac scaffolds. *Sci Rep* 2019; 9: 1–13.
26. Basiri A, Farokhi M, Azami M, et al. A silk fibroin/decellularized extract of Wharton's jelly hydrogel intended for cartilage tissue engineering. *Prog Biomater* 2019; 8: 31–42.
27. Lu H, Hoshiba T, Kawazoe N, et al. Comparison of decellularization techniques for preparation of extracellular matrix scaffolds derived from three-dimensional cell culture. *Biomed Mater Res A* 2012; 9: 2507–2516.
28. Quint C, Kondo Y, Manson RJ, et al. Decellularized tissue-engineered blood vessel as an arterial conduit. *Proc Natl Acad Sci U S A* 2011; 108: 9214–9219.
29. Wu J, Ding Q, Dutta A, et al. An injectable extracellular matrix derived hydrogel for meniscus repair and regeneration. *Acta Biomater* 2015; 16: 49–59.
30. Yusof F, Sha'ban M and Azhim A. Development of decellularized meniscus using closed sonication treatment system: potential scaffolds for orthopedics tissue engineering applications. *Int J Nanomedicine* 2019; 14: 5491–5502.
31. Muiznieks LD and Keeley FW. Molecular assembly and mechanical properties of the extracellular matrix: a fibrous protein perspective. *Biochim Biophys Acta Mol Basis Dis* 2013; 1832: 866–875.

32. Kubow KE, Vukmirovic R, Zhe L, et al. Mechanical forces regulate the interactions of fibronectin and collagen I in extracellular matrix. *Nat Commun* 2015; 6: 1–12.
33. Reese SP, Underwood CJ and Weiss JA. Effects of decorin proteoglycan on fibrillogenesis, ultrastructure, and mechanics of Type I collagen gels. *Matrix Biol* 2014; 32: 1–24.
34. Mattson JM, Turcotte R and Zhang Y. Glycosaminoglycans contribute to extracellular matrix fiber recruitment and arterial wall mechanics. *Biomech Model Mechanobiol* 2018; 16: 213–225.
35. Gheduzzi D, Guerra D, Bochicchio B, et al. Heparan sulphate interacts with tropoelastin, with some tropoelastin peptides and is present in human dermis elastic fibers. *Matrix Biol* 2005; 24: 15–25.
36. Wu WJ, Vrhovski B and Weiss AS. Glycosaminoglycans mediate the coacervation of human tropoelastin through dominant charge interactions involving lysine side chains. *J Biol Chem* 1999; 274: 21719–21724.
37. Kalbitzer L, Franke K, Möller S, et al. Glycosaminoglycan functionalization of mechanically and topologically defined collagen I matrices. *J Mater Chem B* 2015; 3: 8902–8910.
38. Henninger HB, Valdez WR, Scott SA, et al. Elastin governs the mechanical response of medial collateral ligament under shear and transverse tensile loading. *Acta Biomater* 2015; 25: 304–312.
39. Hosseinzadeh S, Soleimani M, Farahani EV, et al. Detailed mechanism of aniline nucleation into more conductive nanofiber. *Synth Met* 2015; 209: 91–98.
40. Toledano-Thompson T, Loría-Bastarrachea MI and Aguilar-Vega MJ. Characterization of henequen cellulose microfibers treated with an epoxide and grafted with poly(acrylic acid). *Carbohydr Polym* 2005; 62: 67–73.
41. Samouillan V, Delaunay F, Dandurand J, et al. The use of thermal techniques for the characterization and selection of natural biomaterials. *J Funct Biomater* 2011; 2: 230–248.
42. Ouyang L, Yao R, Zhao Y, et al. Effect of bioink properties on printability and cell viability for 3D bioplotting of embryonic stem cells. *Biofabrication* 2016; 8: 035020.
43. Göhl J, Markstedt K, Mark A, et al. Simulations of 3D bioprinting: predicting bioprintability of nanofibrillar inks. *Biofabrication* 2018; 10: 034105.